Hindawi
International Journal of Rotating Machinery
Volume 2024, Article ID 4097526, 9 pages
https://doi.org/10.1155/2024/4097526

Research Article

Influence of Inlet and Outlet Area Ratio on Intake Port Flow Capacity

Jingmin Rui,[1] **Jiangjiang Li**,[1] **Chenhong Feng**,[1] **Zhongjie Shi**,[2] **and Dehai Li**[3]

[1]*Tianjin Vocational Institute, Tianjin, China*
[2]*Beijing Institute of Technology, Beijing, China*
[3]*Tianjin Linghai Weiye Technology Development Co., Ltd, Tianjin, China*

Correspondence should be addressed to Zhongjie Shi; shizhongjie@bit.edu.cn

Received 28 November 2023; Revised 31 January 2024; Accepted 24 February 2024; Published 19 March 2024

Academic Editor: Phillip Ligrani

The flow capacity of the intake port has a great influence on the charging efficiency of the internal combustion engine, affecting the engine's performance, so it is critical to improve the intake port flow capacity. In this paper, the intake port numerical model was established, and the influence of the inlet and outlet area ratio on intake port flow capacity was studied. The results show that, under the same condition of relative pressure difference, the intake port discharge coefficient increases sharply and then slowly with an increase in area ratio. Under the same condition of area ratio, the discharge coefficient is only determined by relative pressure difference and decreases with an increase of relative pressure difference when the inlet and outlet area ratio > 1. The optimal area ratio decreases and then converges with an increase in relative pressure difference. When the intake port is designed, the optimal area ratio under the working condition of a smaller relative pressure difference should be applied in order to ensure the discharge coefficient is optimal under all working conditions.

1. Introduction

With the environmental situation getting worse, the emission has become the internal combustion engine (IC engine) focus, which requires emission to be as important as performance [1]. The engine is developing towards the direction of high supercharging and high injection pressure, which can increase the fuel injection quantity and power density under the same displacement [2–5]. However, for high power-density engine, the cycle air inflow is one of the main factors that restrict the power increase. The cycle air inflow has a great relationship with the performance of the intake and exhaust system which is mainly determined by intake port flow capacity. Thus, it is critical for the intake port to be well-designed.

Many researches on intake port optimization design were conducted by scholars.

How the intake port affects the swirl flow of a single-cylinder diesel engine was studied by Aljarf et al. [6], and a more stable swirl was acquired by reducing the aperture of the helical port. Three cylinder heads with varied intake port shapes were experimentally investigated by Kim et al. [7] to evaluate intake flow structures and their influence on near-top dead center flow fields and turbulence distributions, and the results show that a straighter intake port producing a more lateral flow direction results in a larger swinging arc. The profile of the intake port throat was optimized by Verma et al. based on the adjoint method of multiobjective [8], in which the airflow movement was strengthened and the flow loss was reduced in the intake port. Fu [9] changed the flow field distribution characteristics of the intake process by installing guide vanes in the intake port which in turn affected the intensity of the intake vortex in the cylinder, resulting in a 47.62% increase in the vortex ratio. The flow capacity of the intake port designed based on the relationship was significantly improved. Lu [10] optimized the intake port by expanding the minimum cross-sectional area, raising the valve recess height, and increasing the intake valve seat diameter, improving the discharge coefficient significantly. The intake and exhaust ports of a four-valve engine were designed by Latheesh et al. using STAR-CCM+ [11], and the flow coefficient and swirl ratio were calculated

for different valve lifts. The results showed that the position of the helical and tangential intake ports had a significant impact on the flow in the cylinder. The gas flow characteristics in the cylinder with different inlet geometries using tomographic PIV technology were studied by Agarwal et al. [12]. The PIV results were validated through combustion and particle emission tests, and the results showed that the combustion effect of a single helical port engine was the best, with a single tangential inlet engine emitting more particles. The cross-sectional dimensions of the inlet and outlet at the spiral section of the intake port, as well as the internal and external radius structure of the volute, were modified by Wang et al. [13] and numerically simulated. Through simulation, it was found that the flow coefficient of the improved intake port increased by 4% and the vortex ratio increased by 16.5%. The effects of different inlet structures on the steady-state and transient roll flow intensity and combustion performance in the cylinder were studied by Lou et al. [14]. The results showed that a higher roll flow ratio will improve the fuel-air mixture in the cylinder, increase the average turbulent kinetic energy in the cylinder at ignition time, and affect the performance of gasoline engines. The inlet with rolling flow characteristics was optimized and designed by Tang et al. [15]. Research has shown that the rolling flow inlet has low cyclic fluctuations, good combustion stability, and a higher tolerance for exhaust gas recirculation (EGR) rate, which is beneficial for reducing exhaust temperature. For the problem of low high-speed power performance of a certain engine, Yong et al. improved the intake port structure to increase its flow coefficient [16], resulting in an increase in engine power of 15.59%, an increase in torque of 11.92%, and a decrease in fuel consumption rate of 3.33%.

In summary, many scholars have made some achievements in the optimization design of intake port, showing the importance of intake port.

High-power density engines aim to achieve a predetermined power output with the most compact structure. Only by obtaining the influence law of the inlet and outlet areas ratio on the flow capacity of the intake port can the minimum inlet area be obtained while ensuring the flow capacity of the intake port, thereby maximizing the compact size of the cylinder head. At present, no scholars have systematically studied the impact of the inlet and outlet area ratio on the flow capacity of the intake port. Therefore, it is necessary to conduct systematic research to provide theoretical guidance for intake port design.

2. Method

The research in the paper was conducted through the steady CFD method.

2.1. Establishment of Intake Port Model. An intake port numerical model was established based on the actual intake port. The numerical model consisted of a regulator box, intake port, intake valve, valve seat, and cylinder line (shown in Figure 1). Pressure boundary conditions are adopted at the inlet and outlet, where the total pressure was set at the inlet and static pressure was set at the outlet. The numerical pressure difference was consistent with the test pressure difference. The k-ε turbulence model was set as the turbulence model, the standard wall function was used in the near wall region, and the no-slip adiabatic wall was adopted. The residual values of pressure, momentum, and turbulent kinetic energy were 10^{-4}.

2.2. Validation of Grids. The base grid size was 4 mm, and the grids at the intake port were refined. Different refined sizes are shown in Table 1.

The valve lift was 8 mm, the inlet total pressure was 100 kPa, and the outlet static pressure was 95 kPa. The trend of the discharge coefficient (the discharge coefficient is a dimensionless parameter used to characterize the flow capacity of the intake and exhaust ports) and computing time with grid number is shown in Figure 2.

The discharge coefficient can be expressed as follows:

$$c = \frac{m}{m_t}, \tag{1}$$

where m is the actual mass flow rate and m_t is the theoretical mass flow rate.

The theoretical mass flow rate m_t can be described as follows [17]:

$$m_t = A \cdot \rho_0 \sqrt{\frac{2k}{k-1}\frac{p_0}{\rho_0}\left[\left(\frac{p}{\rho_0}\right)^{2/k} - \left(\frac{p}{\rho_0}\right)^{k+1/k}\right]}, \tag{2}$$

where k is the adiabatic index, p_0 is the stagnation pressure, ρ_0 is the stagnation density, p is the outlet pressure, and A is the outlet area.

The discharge coefficient is calculated as follows: First, the actual mass flow rate m is obtained through test or simulation. Then, the theoretical mass flow rate m_t is calculated from Eq. (2) (where the stagnation parameters p_0 and ρ_0 are the values used in the test or simulation). Finally, the discharge coefficient c is obtained by the ratio of m to m_t.

The discharge coefficient converged gradually with the decrease of grid size. When the refined grid size was larger than 1 mm, the discharge coefficient kept constant, but the computing time increased sharply. Considering the calculation error and computing time, the refinement size of 1 mm was adopted.

2.3. Verification of Intake Port Numerical Model. It has become an important method of IC engine research to evaluate the intake port flow characteristics through steady flow test [18–20]. In order to verify the applicability of the intake port numerical model, the discharge coefficient was obtained through a steady flow test. The schematic diagram of the test system is shown in Figure 3.

The actual mass flow rate of the intake port with different valve lifts was measured under a 5 kPa constant pressure difference. Then the discharge coefficients were calculated by the methodology in reference [17], details of the calculation methodology for discharge coefficient can be found in Section 2.2. These calculation results are the "Test results"

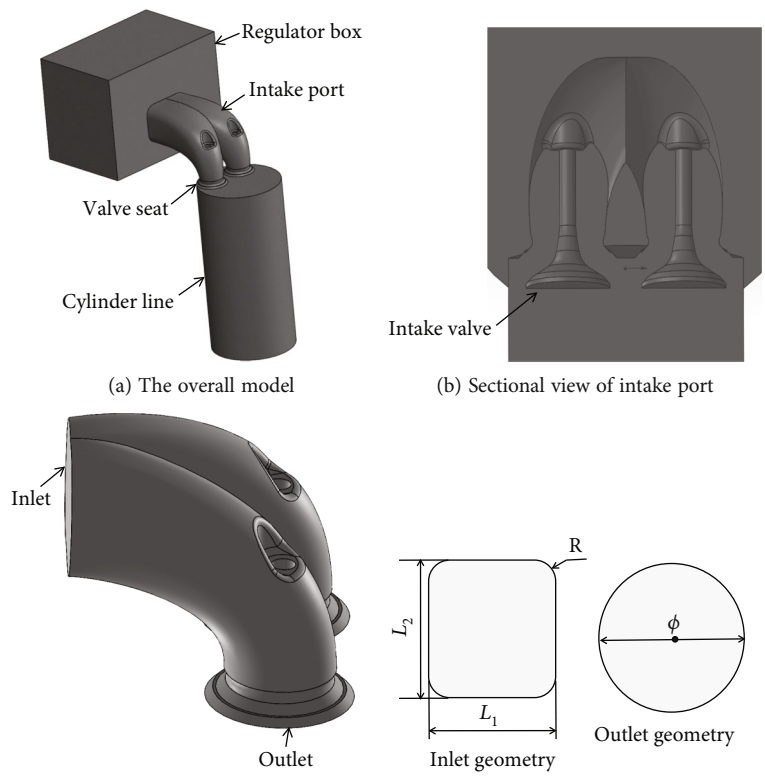

(a) The overall model (b) Sectional view of intake port

(c) The inlet and outlet of the intake port (d) Inlet and outlet geometry

Figure 1: Intake port numerical model.

Table 1: Scheme of grid refinement.

Scheme	Base size (mm)	Refined size (mm)	Grid number
1	4	4	305231
2	4	2	468732
3	4	1.5	703865
4	4	1	1321534
5	4	0.5	3418412

in Table 2. Finally, the numerical results and test results of the discharge coefficient were compared (shown in Table 2).

As shown in Table 2, the numerical discharge coefficients were consistent with test discharge coefficients, and the maximum error is 7.96% < 10%. It was indicated that the intake port numerical model that was established was accurate and reliable. The established model can be used to expand research.

3. Influence of Inlet Area on Intake Port Flow Capacity

3.1. Influence of Inlet and Outlet Area Ratio on Intake Port Flow Capacity under Constant Pressure Difference. Based on the model above, the intake port discharge coefficients were simulated with different inlet and outlet area ratios. The valve lift was 8 mm, the intake total pressure was 300 kPa, and the pressure difference was 90 kPa. The inlet and outlet area ratio was defined as $K = A_{in}/A_{out}$, where A_{in} is the inlet area of the intake port, A_{out} is the outlet area of the intake port, A_{out} usually selects the area at the throat of the valve seat, and the outlet geometry is circular, as shown in Figure 1(d). The simulation results are shown in Figure 4.

It can be seen that the discharge coefficient increases sharply and then slowly with the increase of K. The result was analyzed with the total pressure field, as shown in Figure 5.

When the inlet area is small, the throttling effect is obvious, and the local resistance loss is significant at the inlet. With the increase of inlet area, the inlet local resistance loss decreases obviously, and the discharge coefficient increases. It can be seen from Figure 5(c) that the inlet total pressure has been high pressure when $K > 1$, indicating that the main loss has become the internal flow loss instead of the inlet local resistance loss. The intake port flow loss mainly includes friction drag loss, corner separation loss, and secondary flow loss.

The friction drag loss can be estimated as follows:

$$p_f = \lambda \cdot \frac{l}{d} \cdot \frac{\rho \bar{v}^2}{2}. \tag{3}$$

The secondary flow strength can be estimated by Dean number which is expressed as follows [21]:

$$D_e = \frac{\rho \cdot \bar{v} \cdot d}{\mu} \sqrt{\frac{d}{2R}}, \tag{4}$$

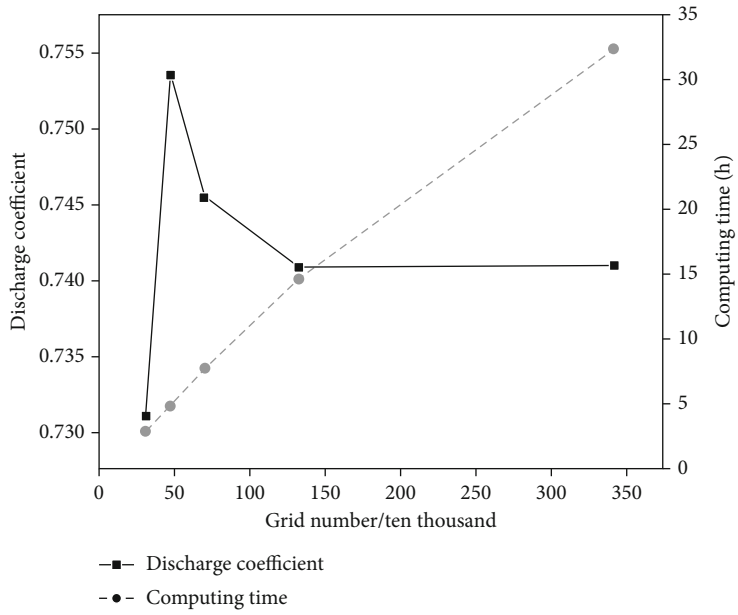

Figure 2: Trend of discharge coefficient and computing time with grid number.

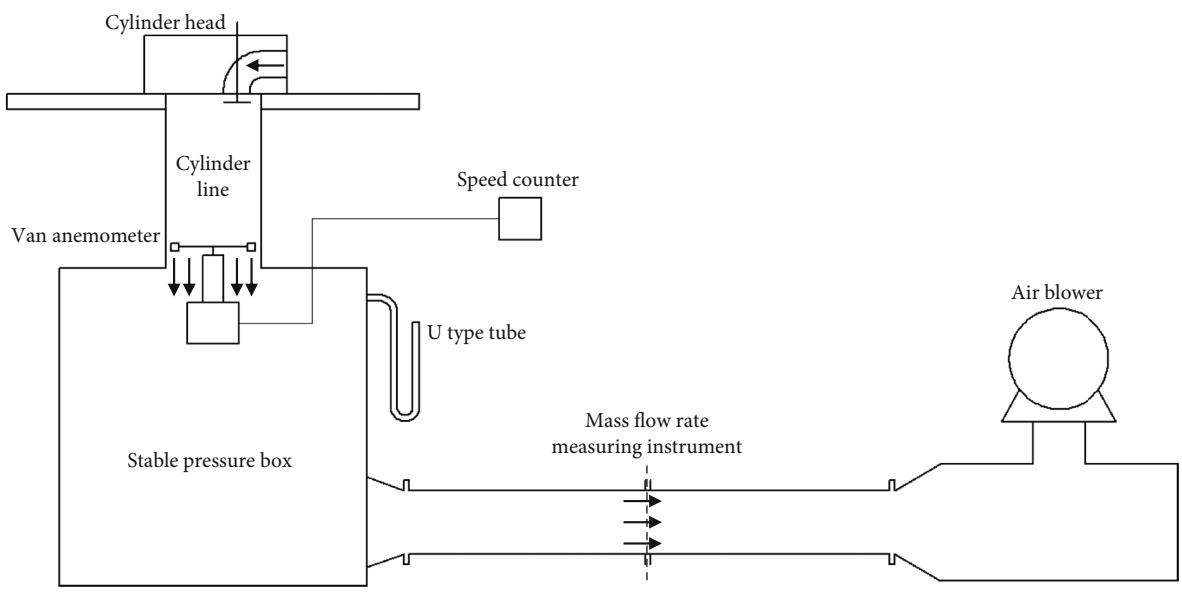

Figure 3: Schematic diagram of steady flow test system.

where λ is the friction drag loss coefficient, which can be calculated by the Nicholas formula [22]. l is the length of the pipeline, d is the diameter of the pipeline, $\bar{v}$ is the fluid average velocity of the pipeline, ρ is the fluid density, μ is the fluid hydrodynamic viscosity, and R is the curvature radius at the reference section.

Due to the fact that under the same structural parameters, the flow resistance in a curved pipe decreases with the decrease of flow velocity, and the flow resistance in a curved pipe mainly comes from flow separation, it can be inferred that the separation loss decreases with the decrease of flow velocity.

According to the continuity equation $\rho vA = \text{const}$, the inlet flow velocity is inversely proportional to the inlet area. With the increase of inlet area, the inlet flow velocity decreases sharply and then slowly, making the friction drag loss, separation loss, and secondary flow loss all decrease sharply and then slowly. So the internal total flow loss decreases, and the discharge coefficient increases sharply and then slowly.

3.2. Influence of Working Condition on the Optimal Inlet and Outlet Area Ratio. In this section, the trend of intake port discharge coefficient with inlet and outlet area ratio was

Table 2: Verification result of intake port numerical model.

Pressure different (kPa)	Valve lift (mm)	Discharge coefficients		
		Test result	Numerical result	Error (%)
5	2	0.201	0.217	7.96
	3	0.293	0.314	7.17
	4	0.391	0.411	5.12
	5	0.453	0.474	4.55
	6	0.528	0.557	5.45
	7	0.601	0.631	5.04
	8	0.712	0.741	4.05

Note: error = (numerical result − test result)/test result × 100%.

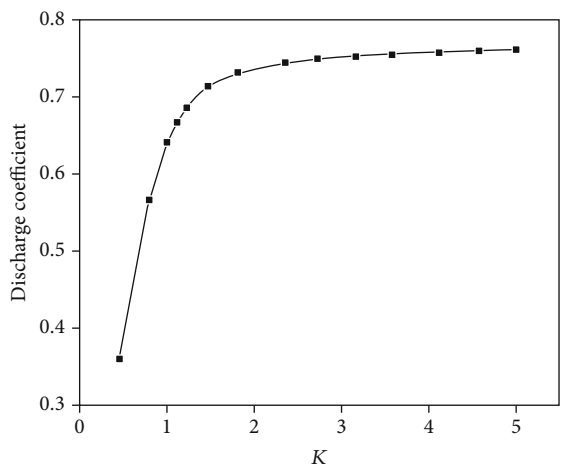

Figure 4: Trend of discharge coefficient with different inlet and outlet area ratios.

studied under different working conditions. Then, the influence of working condition on the optimal inlet and outlet area ratio was obtained.

First, qualitative analysis was carried out.

The Bernoulli equation of compressible and ideal conditions is

$$\frac{k}{k-1}\cdot\frac{p}{\rho}+\frac{{v_t}^2}{2}=\frac{k}{k-1}\cdot\frac{p_0}{\rho_0}, \tag{5}$$

where k is the adiabatic index, v_t is the theoretical velocity, p_0 is the stagnation pressure, ρ_0 is the stagnation density, p is the outlet pressure, and ρ is the outlet density.

Assume that the intake port flow process is adiabatic and isentropic. The isentropic process equation is

$$\frac{p}{\rho^k}=\text{const.} \tag{6}$$

The outlet theoretical velocity can be calculated based on Eqs. (5) and (6).

$$v_t=\sqrt{\frac{2k}{k-1}\frac{p_0}{\rho_0}\left[1-\left(\frac{p}{p_0}\right)^{k-1/k}\right]}. \tag{7}$$

The relative pressure difference (RPD) was defined as

$$p_{re}=\frac{p_0-p}{p_0}. \tag{8}$$

Equation (7) can be changed to Eq. (9) by introducing Eq. (8).

$$v_t=\sqrt{\frac{2k}{k-1}\frac{p_0}{\rho_0}\left[1-(1-p_{re})^{k-1/k}\right]}. \tag{9}$$

The stagnation pressure and the stagnation density are suitable for the ideal gas law.

$$\frac{p}{\rho}=RT, \tag{10}$$

where R is the ideal gas constant and T is the gas thermodynamic temperature.

Because the stagnation temperature in this research was fixed at normal temperature, so that

$$\frac{p_0}{\rho_0}=\text{const.} \tag{11}$$

It can be seen from Eqs. (9) and (11) that the theoretical velocity is only determined by RPD.

The Bernoulli equation of the compressible and actual condition is

$$\frac{k}{k-1}\cdot\frac{p}{\rho}+\frac{{v_a}^2}{2}+\varepsilon\frac{{v_t}^2}{2}=\frac{k}{k-1}\cdot\frac{p_0}{\rho_0}, \tag{12}$$

where v_a is the actual velocity and ε is the energy loss coefficient that is based on the theoretical velocity v_t.

The discharge coefficient is defined as the ratio of actual mass flow rate and theoretical mass flow rate. For the same working condition of a pipe, the actual boundary condition is the same as the theoretical boundary condition, so that the outlet area, the outlet pressure, and the outlet density under actual condition are the same as those under theoretical condition. Therefore, the discharge coefficient can be described as

$$c=\frac{m}{\dot{m}}=\frac{A_{\text{out}}\cdot\rho_{\text{out}}\cdot v_a}{A_{\text{out}}\cdot\rho_{\text{out}}\cdot v_t}=\frac{v_a}{v_t}. \tag{13}$$

Equation (13) can be changed to Eq. (14) by introducing Eqs. (5) and (12).

$$c=\sqrt{1-\varepsilon}. \tag{14}$$

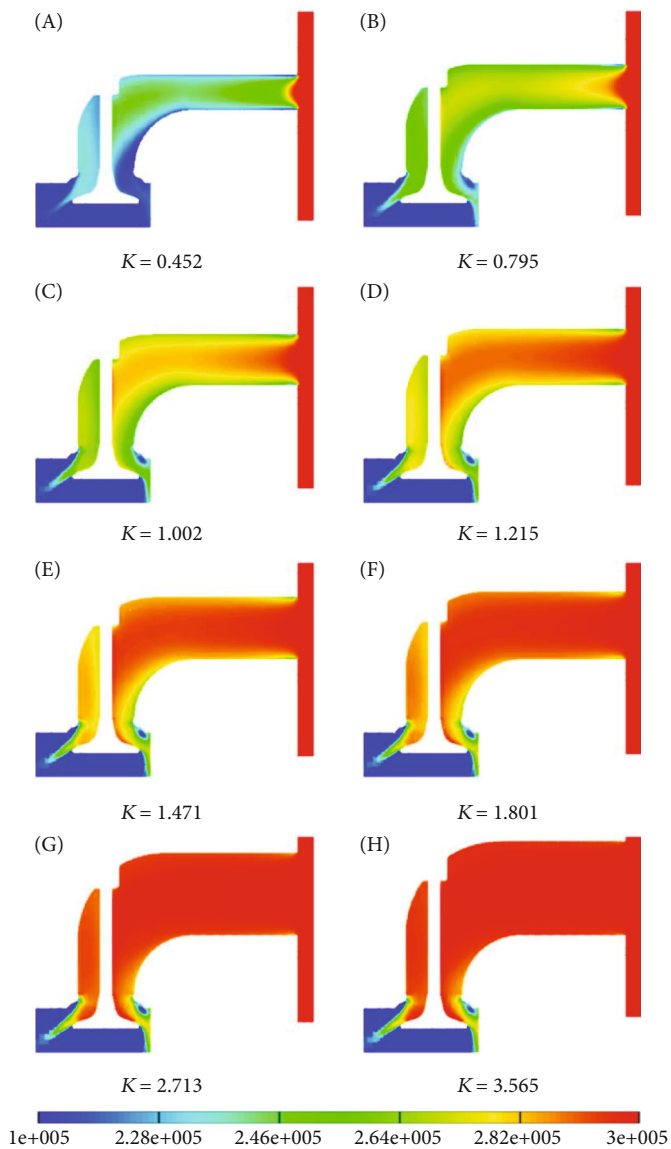

Figure 5: Total pressure field.

It can be seen from Eq. (14) that the discharge coefficient is only determined by the energy loss coefficient which is relative to the structure parameter and Reynolds number [23, 24]. In this research, the structure of the intake port was determined by the inlet and outlet area ratio, and the Reynolds number was determined by the gas velocity (that is RPD). So it can be predicted that the discharge coefficients are the same under the same area ratio and RPD. The prediction was verified by simulating the intake port discharge coefficient with different inlet and outlet area ratios under different intake pressure and RPD conditions. The intake pressure was 100 kPa, 300 kPa, and 500 kPa, and the RPD were 0.1 and 0.5. The numerical results are shown in Figure 6.

The maximum error was defined as the error between the maximum discharge coefficient and the minimum discharge coefficient under the same area ratio and RPD. The calculation equation is as follows:

$$\frac{c_{\max} - c_{\min}}{c_{\max}} \times 100\%. \tag{15}$$

It can be seen that the intake port discharge coefficients with the same area ratio are basically the same under different intake pressures and the same RPD condition. The maximum errors were all less than 3%, indicating that the prediction is correct. So in further research, only RPD was considered in working condition.

For the diesel engine, the pressure at the end of the intake process is about 0.85~0.95 of atmospheric pressure [25], that is, the RPD at the end of the intake process is 0.05~0.15. However, with the improvement of the turbocharging ratio and speed of the diesel engine, the intake port pressure difference is also increased. According to some researches, the maximum intake RPD can reach 0.37 in a high-power diesel engine [26]. So in order to cover all the working conditions, the RPD in this study was 0.05~0.5,

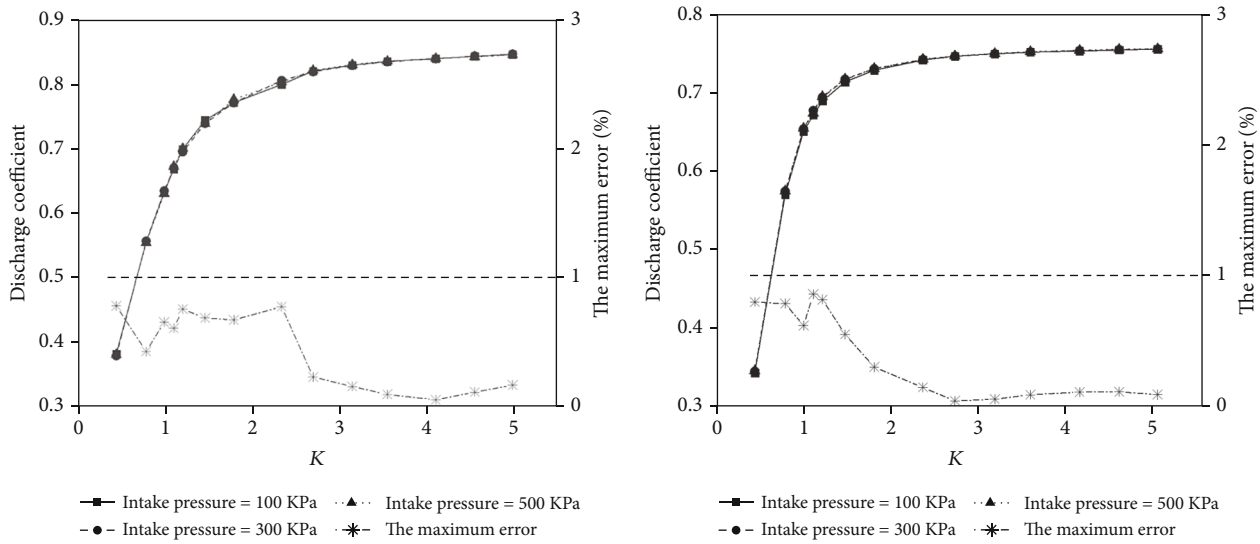

(a) RPD = 0.1

(b) RPD = 0.5

Figure 6: Trend of discharge coefficients with different intake pressure and RPD.

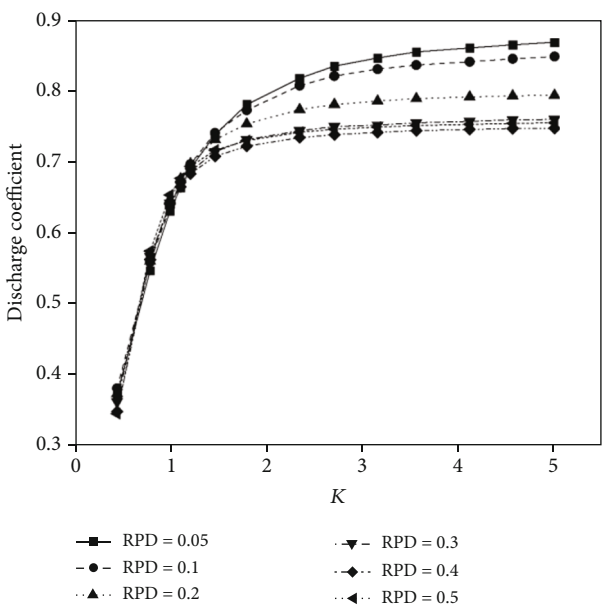

Figure 7: Trend of discharge coefficients with different inlet and outlet area ratios and RPD.

and the flow coefficient under different inlet and outlet area ratios is calculated. The results are shown in Figure 7.

It can be seen that under the same RPD condition, the intake port discharge coefficients all increase sharply and then slowly with the increase of inlet and outlet area ratio. When $K < 1$, the discharge coefficients of the same area ratio and different RPD are basically the same. It is because the energy loss coefficient is determined by structure when $K < 1$. Therefore, the area ratio is the same, the energy loss coefficient is basically the same, and the discharge coefficient is the same. When $K > 1$, the discharge coefficient of the same area ratio decreases with the increase of RPD. It is because the influence of flow velocity on the energy loss coefficient is significant when $K > 1$, the larger the flow velocity is, the larger the energy loss coefficient is. Therefore, the discharge coefficient is smaller under larger RPD condition.

The optimal discharge coefficient of some RPD was defined as 95% of the maximum discharge coefficient of the same RPD. The corresponding area ratio was taken as the optimal inlet and outlet area ratio (K_{opt}). The trend of K_{opt} with RPD is shown in Figure 8.

As can be seen, with the increase of RPD, the optimal area ratio K_{opt} decreases first and then keeps constant when RPD > 0.4. The analysis is as follows:

According to the result above, the outlet flow velocity is constant under constant RPD. And with the increase of the inlet area, the valve seat area which is the intake port outlet area is constant. So under constant RPD condition, the outlet area and flow velocity are both constant so that the outlet local resistance loss keeps constant with the increase of inlet area; however, because of the decrease of the inlet local resistance loss and internal flow loss both decrease, the outlet local resistance loss increases in proportion to total energy loss. According to reference [19], when the inlet area is larger than the outlet area, the valve seat local resistance loss can account for more than 80% of the total energy loss, and the proportion increases with the increase of RPD. The greater the proportion is, the smaller the improvement range of the discharge coefficient is. Therefore, the energy loss under larger RPD is easier to decrease to the limit with the increase of area ratio, so that the optimal area ratio is relatively small.

Based on the velocity field, when the RPD > 0.4, the Mach number of outlet velocity had reached 0.886, which is basically close to the sonic speed. According to the critical pressure ratio, when the RPD > 0.472, the outlet flow velocity would reach sonic velocity and would not increase with the increase of RPD. So when the RPD > 0.4, the outlet flow

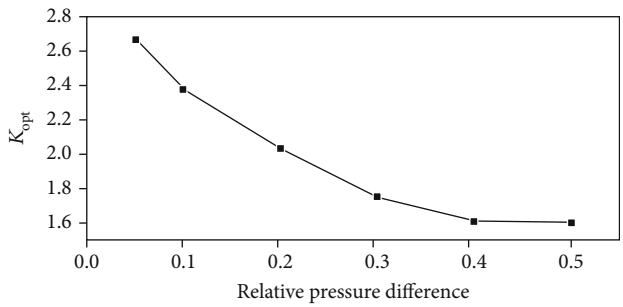

Figure 8: Trend of the optimal inlet and outlet area ratio with RPD.

velocity only increased slightly. As can be seen from the results above, the discharge coefficient of the intake port with the same area ratio was mainly determined by flow velocity which is determined by RPD. So when PRD > 0.4, with the further increase of RPD, the flow velocity basically kept constant and the discharge coefficient of the intake port with the same area ratio basically kept constant so that the optimal area ratio K_{opt} kept constant.

Based on the above research results, when the intake port is designed, in order to make the discharge coefficient all optimal under all the working conditions, the optimal inlet and outlet area ratio under the working condition of smaller RPD should be adopted. For the intake port in this paper, the inlet and outlet area ratio should be $K_{opt} = 2.66$.

4. Conclusion

In this paper, the intake port numerical model was established, and the influence of inlet and outlet area ratio on intake port flow capacity was studied based on AVL-Fire. The results are as follows:

(1) Under constant pressure difference, the discharge coefficient increased sharply and then slowly with the increase of inlet and outlet area ratio

(2) Under constant inlet and outlet area ratio, the discharge coefficients were determined by relative pressure difference, that is, the same relative pressure difference was, the same discharge coefficient was. And when the area ratio $K > 1$, the discharge coefficient decreases with the increase of relative pressure difference

(3) The optimal area ratio K_{opt} decreased first and then kept constant with the increase of relative pressure difference. When the intake port is designed, the optimal inlet and outlet area ratio under the working condition of a smaller relative pressure difference should be adopted. For the intake port in this study, the inlet and outlet area ratio should be $K_{opt} = 2.66$

Suggestions for future research: This study mainly focused on the influence of inlet and outlet area ratio on intake port flow capacity, and the variable was only the inlet area. Subsequently, the internal flow channel geometry of the intake port can be parameterized, combined with the inlet area, to study the coupling influence of the intake port structural parameters on its flow capacity, thereby providing more comprehensive theoretical guidance for the intake port design.

Data Availability

The data used to support the findings of this study are included within the article.

Conflicts of Interest

The authors declare that they have no conflicts of interest.

References

[1] N. I. Masuk, K. Mostakim, and S. D. Kanka, "Performance and emission characteristic analysis of a gasoline engine utilizing different types of alternative fuels: a comprehensive review," *Energy & Fuels*, vol. 35, no. 6, pp. 4644–4669, 2021.

[2] D. Dong, R. Wang, W. Fuxing et al., "Development of a high-power density diesel engine with a heat-insulation coating: application of ultrahigh-pressure fuel injection," *Journal of Energy Engineering*, vol. 149, no. 5, 2023.

[3] F. Millo, A. Piano, B. P. Paradisi, M. R. Marzano, A. Bianco, and F. C. Pesce, "Development and assessment of an integrated 1D-3D CFD codes coupling methodology for diesel engine combustion simulation and optimization," *Energies*, vol. 13, no. 7, 2020.

[4] Y. Xu, *Research on influence law of inlet and exhaust throat on engine performance of high boost ratio engine*, Jiangsu University of Science and Technology, Jiangsu China, 2022.

[5] B. Peter, V. Sudharsan, and B. Mirko, "Subcooled flow boiling in high power density internal combustion engines I: thermal survey measurement campaign," *SAE International Journal of Engines*, vol. 16, no. 1, pp. 17–33, 2023.

[6] A. L. J. A. R. F. Saad, S. I. N. G. H. Hardeep, N. D. I. Z. E. Y. E. Gerard, I. C. H. I. Y. A. N. A. G. I. Mitsuhisa, and S. U. Z. U. K. I. Takashi, "Effect of a dual air inlet port of the 4-valve CI engine on the swirl flow generated at the bottom region of the cylinder using the PIV technique," *Mechanical Engineering Journal*, vol. 8, no. 2, 2021.

[7] K. Dongchan, R. Lingzhe, K. Sanghoon, L. S. Woo, and B. H. Kil, "The effect of intake port shape on in-cylinder flow field and turbulence distribution in a high-tumble production engine with endoscope accesses," *International Journal of Engine Research*, vol. 24, no. 9, pp. 4154–4168, 2023.

[8] I. Verma, C. Hill, and M. Xu, "Multi-objective adjoint optimization of flow-bench port geometry," SAE Technical Paper 2018-01-0772, 2018.

[9] F. Changran, *Simulation of improvements to flow characteristics in diesel intake port by incorporating guide vanes into the intake manifold*, Jilin University, Jilin China, 2020.

[10] Z. Lu, *Airway design improvement and performance experimental study on 493 type diesel engine*, Hunan University, Changsha, 2016.

[11] V. M. Latheesh, P. Parthasarathy, V. Baskaran, and S. Karthikeyan, "Design and CFD analysis of intake port and exhaust port for a 4 valve cylinder head engine," *IOP*

Conference Series: Materials Science and Engineering, vol. 310, article 012122, 2018.

[12] A. A. Kumar, G. Suresh, and S. A. Pratap, "In-cylinder air-flow characteristics of different intake port geometries using tomographic PIV," *Physics of Fluids*, vol. 29, no. 9, article 095104, 2017.

[13] G. Wang, W. Yu, X. Li, and R. Yang, "Influence of fuel injection and intake port on combustion characteristics of controllable intake swirl diesel engine," *Fuel*, vol. 262, article 116548, 2020.

[14] L. Diming, X. Pan, F. Liang, Z. Xiaomao, S. Yafeng, and S. Jian, "Effect of inlet structure on tumble intensity and combustion process of hybrid gasoline-direct-injection engine," *Journal of Tong Ji University*, vol. 50, no. 2, pp. 264–272, 2022.

[15] T. Zhigang, Y. Pan, L. Wei, L. Zhe, L. Liang, and L. Hongzhe, "Investigation on the influence of intake port flow pattern on the performance of a NG engine," *Transactions of CSICE*, vol. 41, no. 5, pp. 435–441, 2023.

[16] Z. Yong, Y. Gao, G. Kui, W. Xiaoyong, and C. Minxu, "Multi-objective optimization and experimental study of gasoline engine power performance," *Vehicle Engine*, vol. 5, pp. 35–40, 2023.

[17] L. Fushui, K. Ning, Y. Xu, and L. Yikai, "Discharge coefficient evaluation and steady flow characteristics for intake port of turbocharged diesel engine," *Transactions of the Chinese Society for Agricultural Machinery*, vol. 48, no. 6, pp. 341–348, 2017.

[18] H. Xu, L. Nan, and L. Zhenming, "Simulation study on the influence of inlet structure on intake process," *Internal Combustion Engines*, vol. 6, pp. 56–59, 2019.

[19] Z. Haifeng, G. Lu, S. Tansu, D. Xiaohui, and Z. Gao, "Research on performance optimization of an engine port," *Internal Combustion Engine & Parts*, vol. 24, pp. 5–8, 2023.

[20] M. Ichiyanagi, E. Yilmaz, K. Hamada, T. Hara, W. Anggono, and T. Suzuki, "Experimental investigation of the in-cylinder flow of a compression ignition optical engine for different tangential port opening areas," *Energies*, vol. 16, no. 24, p. 8110, 2023.

[21] L. Tangjing, Q. Wang, and Z. He, "Numerical study of secondary flow phenomenon of viscoelastic fluid in curved channel," *Light Industry Machinery*, vol. 40, no. 1, pp. 1–6, 2022.

[22] G. Keting, *Engineering Fluid Dynamics*, Science Press, Jiangsu China, 3rd edition, 2020.

[23] Z. Yue, *Numerical simulation on local resistance based on CFD*, Northeast Petroleum University, Daqing China, 2011.

[24] C. Zhao, *The numerical simulation of local head losses in common pipes*, Tianjin University, Tanjin, 2008.

[25] L. Shenghua, *Internal Combustion Engine*, Machinery Industry Press, Beijing China, 4th edition, 2017.

[26] B. Wang, *Simulation study of high pressure difference inlet port based on AVL-fire*, North University of China, Taiyuan China, 2020.